REVIEW ARTICLE   OPEN

Recent advanced applications of ion-gel in ionic-gated transistor

Depeng Wang[1], Shufang Zhao[1], Ruiyang Yin[1], Linlin Li[1], Zheng Lou [1]✉ and Guozhen Shen [1]✉

Diversified regulation of electrons have received much attention to realize a multi-functional transistor, and it is crucial to have a considerable control over the charge carriers in transistors. Ionic gel, as the dielectric material in transistors, facilitates a large capacitance, and high induced-carrier concentrations. This review presents the recent progress in ionic-gated transistors (IGTs) that have good mechanical stability as well as high physical and chemical stability. We first briefly introduce the various applications of IGTs in sensors, neuromorphic transistors, organic transistor circuits, and health detection. Finally, the future perspectives of IGTs are discussed and some possible solutions to the challenges are also proposed.

INTRODUCTION

In the past decade, with the rapid development of the Internet of Things and consumer electronics, human demand for high performance, portability, and wear-ability pushed the upgrade of transistor integration density. However, due to the tunneling effect and other problems, this trend of continuing to use Moore's Law will inevitably slow down. Therefore, in order to develop more promising integrated circuit applications in the post-Moore era, tremendous efforts are being invested to develop materials and structures aspects to improve the performance of field-effect transistors(FETs)[1–3]. Many inorganic materials with high dielectric constant have been extensively studied, like HfO_2[4] and Al_2O_3[5,6]. Unfortunately, the high dielectric constant causes the carrier mobility decreased in the transistor because of Fröhlich polarons[7].

Meanwhile, a kind of transistor with ionic gate, ionic-gated transistors (IGTs) has attracted widespread attention owing to its large capacitance, high carrier-inducing ability, and low operating voltage[8]. The function of IGT is similar to that of traditional MOSFET, and the channel current of IGT is also controlled by the gate voltage[9]. The difference is that IGT replaces the dielectric material with the electrolyte material. When a negative voltage is applied to the gate electrode, cations in the electrolyte accumulate at the gate/electrolyte interface under the electrostatic mechanism, forming a capacitor layer C_{ge} that is opposite to the charge of the gate electrode. At the same time, a capacitor layer C_{es} is also formed at the channel layer/electrolyte interface. Since the layer spacing of the two significant parallel plate capacitors is ~1 nm, the capacitance effect is significantly greater than that of general insulating layer materials[8,10]. This type of IGT based on an electric double layer is also named electric double layer transistor (EDLT). In addition, the channel layer material may also allow electrolyte ion implantation, thereby causing electrochemical doping[11]. Due to the typical EDL effect, the large surface capacitance allows the IGT to operate well at a relatively low operating voltage[12] and maintain good switching performance[13]. Nowadays, the research of ion-gated transistors is booming in various disciplines, and the ion materials include electrolyte solutions[14–16] and ionic liquids[7,17–19] with liquid fluidity; as well as ions/proton-conducting polymers[20–22], and inorganic materials[23].

As a kind of electrolyte, ionic gel not only has good physical/chemical stability, but also has the characteristics of flexibility, lightweight, and transparency. Therefore, in the field of wearable electronic devices, IGT has demonstrated unquestionable adaptability, portability, and functionality. These characteristics have aroused the research enthusiasm for the application of ionic-gel to IGT. In addition, it is well known that the nervous system controls the activities of the human body through electrical and chemical signals. IGT has the potential advantage of being compatible with biological signals due to its similar electrical characteristics, structure flexible, and low toxic. IGT has also been studied in the context of neuromorphology, memory, and synaptic devices, and is expected to be applied in the field of artificial intelligence[24–27].

In this review, we will briefly list material choices, and introduce the conventional and emerging applications of IGTs in flexible electronics. Recent articles on the sensing function, neuromorphic, and IC function of IGTs will be discussed in detail. The schematic device structure of IGT applications is summarized in Fig. 1. Finally, the future development and problems of IGT sensing and neuromorphic systems are summarized in Section 6.

MATERIALS ASPECT OF IONIC-GEL-GATED TRANSISTOR

Tremendous efforts have been invested in IGTs, and the dielectric materials consist of polymer electrolytes, polyelectrolytes, ILs, ionic gels, and inorganic nanogranular materials[28]. Polymer electrolytes and polyelectrolytes have shown an excellent capacitance performance, whereas, they also exhibit a slow ion migration, which limits the application of IGTs in high-speed electronic devices[20,29]. ILs have good gating functions and faster responses; however, their intrinsic liquid state hinders the use of ILs in practical devices[7]. Therefore, as an alternative to ILs, ionic gels solve the problem by combining polymer mechanical compatibility and swift switching response. An ionic gel is a semi-solid compound that retains charge owing to the insertion of an IL into the polymer during the drying stage. The colloidal particles in the mixture prevent it from curing completely, but are in the form of a gel. Due to their excellent chemical stability and transmittance, these materials are also widely used as battery electrolyte materials. As a result, they are also named as electrolyte gated

[1]State Key Laboratory for Superlattices and Microstructures, Institute of Semiconductors, Chinese Academy of Sciences & Center of Materials Science and Optoelectronic Engineering, University of Chinese Academy of Sciences, Beijing, China. ✉email: zlou@semi.ac.cn; gzshen@semi.ac.cn
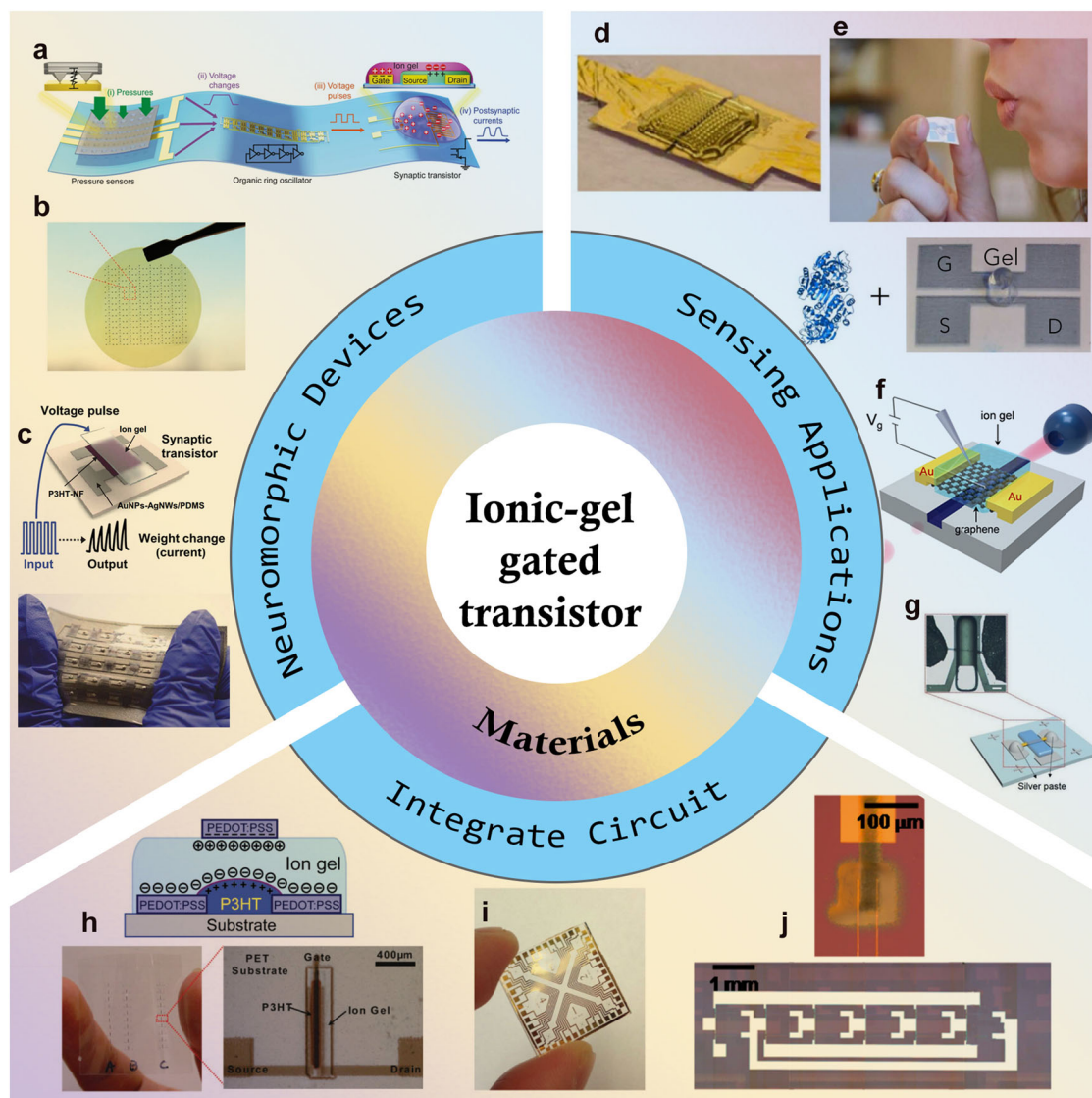
Fig. 1 Prospective applications of ionic gel-based electronics. a An artificial afferent nerve made of pressure sensors, an organic ring oscillator, and a synaptic transistor. Reproduced with permission[127]. Copyright 2018, Elsevier. **b** Optical photo of Ionic-gel transistor. Reproduced with permission[118]. Copyright 2020, Wiley-VCH. **c** Schematic device structure and demonstration of multiple presynaptic pulses induced synaptic transistor responses[26]. Copyright 2019, Elsevier. **d** A real optical image of the OECT iontronic pressure sensor. Reproduced with permission[84]. Copyright 2021, IEEE. **e** The physical schematic diagram of the transistor-breathalyzer. Reproduced with permission[104]. Copyright 2016, Springer Nature. **f** Schematics of the ionic-gel-integrated optical-transistor modulator. Reproduced with permission[74]. Copyright 2017, American Chemical Society. **g** A diagram of an IGT device using a nanowire as a stress-sensing material. Reproduced with permission[128]. Copyright 2019, Elsevier. **h** Schematic and physical optical photo of a single device used to prepare the inverter. Reproduced with permission[121]. Copyright 2010, Wiley-VCH. **i** A picture of completed IGZO-EGTFT device arrays. Reproduced with permission[129]. Copyright 2015, Springer Nature. **j** Optical picture of a single inverter and the electrode of the substrate before preparation. Reproduced with permission[130]. Copyright 2013, American Chemical Society.

transistors (EGT). In the following section, we describe ILs and the polymer grid used in IGTs.

ILs are generally known as room-temperature molten salt. Owing to the low vapor pressure, high ionic conductivity, and good temperature (up to 350 °C), and chemical stabilities, ILs are more suitable for polymer-in-salt systems. In 1992, since Wilkes et al. prepared 1-ethyl-3-methylimidazole tetrafluoroborate ([EMIM][BF$_4$]) with good stability in the air, the research on ionic liquids has flourished[30]. Ionic gels have a wide selection of anions[31-34], so ionic gels are usually classified according to the types of cations, including quaternary ammonium[35,36], phosphonium[37], Imidazole[38], and pyridine[39], etc. Imidazole-based ionic liquids are widely used in emerging electronic devices due to their generally low melting point and many optional substituents[40,41].

Figure 2 shows the structures of cations and anions conventionally used in IL, and the various properties of IL are determined by the combination of different anions and oxygen ions. Generally, most of the studies on the potential applications of ionic gel have advanced toward electrical and electrochemical devices, including sensors[42], super capacitors[43], batteries[32,39,44-46], actuators[47,48], electrochromic devices[41,49], solar batteries[50,51], FET[52], and optimization of thermoelectric materials using IGTs[22]. The manufacturing method, materials, and performance of the reported nanoscale IGTs are compared in Table 1.

ILs, such as [EMIM][TFSI][53,54], [EMIM][TFSA][55,56], and [BMIM][PF$_6$][57], have been reported to be widely used and have good performance. Cho et al. used a chemically stable ionic liquid, [EMIM] [TFSI], and photocurable mixture material to prepare
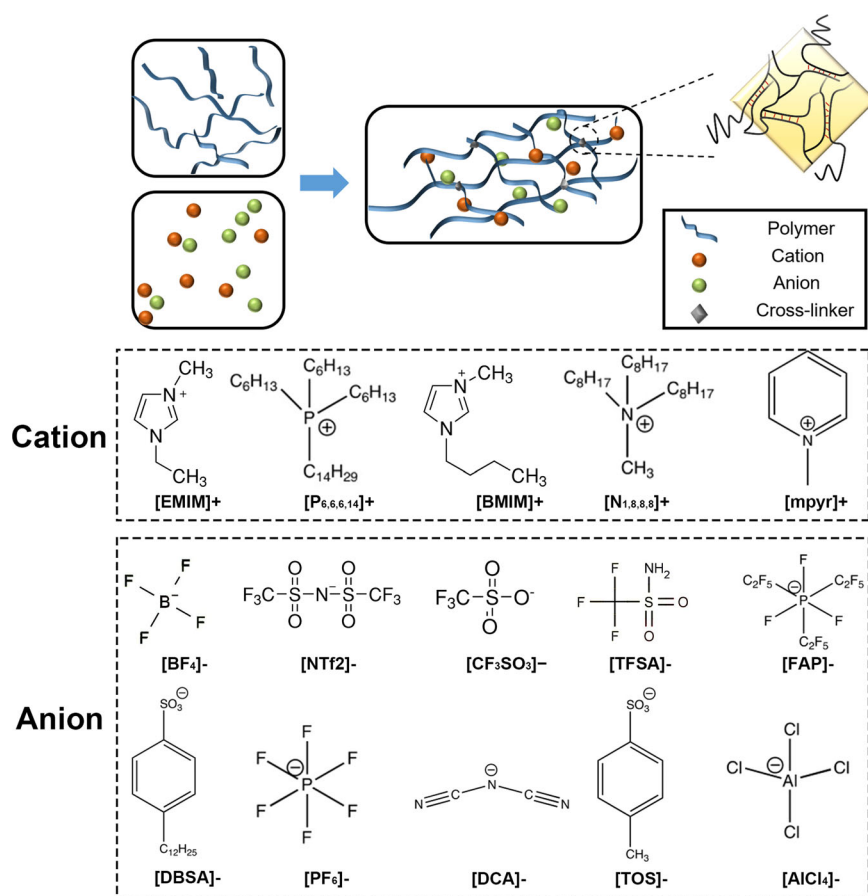
Fig. 2 The type of ionic-gel structure. Three different types of ionic-gel composition structure and main ionic-gel anion and cation types.

patterned graphene transistors under ultraviolet (UV) radiation[58]. The presence of ionic liquid not only maintains stability but also exhibits excellent surface capacitance and polarization response speed. Besides being extremely sensitive to external bending and deformation (GF~389), the system can also implement a large-area, highly integrated array on a flexible substrate for motion detection.

However, for in vivo applications, these ILs have not been proven to be safe. Considering these conditions, Tang et al. reported a biocompatible IGT composed of poly(ε-decalactone)-b-poly(DLlactide)-b-poly(ε-decalactone) (DLD) and $[P_{14}][TFSI]$[37]. The minimum capacitance of the 20% ionic gel could reach approximately $2\,\mu F\,cm^{-2}$, ensuring that the system could be operated under a low voltage. The prepared IGT using P3HT as the channel layer showed good characteristics for printed electronic applications: $1\,cm^2\,V^{-1}\,s^{-1}$ mobility, an I_{on}/I_{off} ratio of 10^5, and low hysteresis. Besides, it showed promising hydrolytic degradation. More recently, Kim et al. reported an ionic gel material made of choline and malic acid as raw materials, and the obtained dielectric layer has good biocompatibility and biodegradability[59].

The flexibility of material selection makes it possible to choose different polymers to prepare ionic-gel gate transistors. For most IGTs, polymer monomers are embedded into ionic solutions composed of polymer molecular segments, and the commonly used materials are mainly self-assembled tri-block and di-block co-polymers, such as poly(styrene-block-ethylene oxideblock-styrene) (SOS)[53,60], poly(ε-decalactone)-b-poly(DL-lactide)-b-poly(ε-deca-lactone) (DLD)[37], and poly(styrene-b-methylmethacrylate-b-styr-ene) (SMS)[61,62].

The first ionic-liquid-based gel used in an organic film transistor was produced by Lee et al.[57] They chose a tri-block co-polymer,

(SOS), as the gel network and dissolved it with 1-butyl-3-methylimidazolium hexafluorophosphate ([BMIM][PF6]) into methylene chloride (Shown in Fig. 3a). Tri-block polymers such as SOS have special structural and chemical properties; the entire structure is divided into two parts: can be dissolved (the middle) and cannot be dissolved (on two sides) in IL. Thus, they are collectively referred to as ABA tri-block polymers. This character-istic makes ABA tri-block co-polymers suitable for the preparation of ionic gels. This easily leads to the design and preparation of an ionic gel that can be utilized to construct various transistors with different requirements. In addition to SOS, other ABA tri-block co-polymers, such as SMS, are also widely used in the preparation of ionic gels[61].

According to application scenarios and preparation processes, many chain polymers are also used to prepare IGTs. A transistor that uses P (VDF-HFP) and a gel gate dielectric layer has the characteristics of easy transfer. There is a transistor using P (VDF-HFP) that can easily transfer the gate insulating layer through a "cut and paste" operation[55]. Except good solvent compatibility, the gel material not only has high tension and structural stability, but also exhibits similar properties to triblock polymers in some specific aspects. For example, PVA, (P(VDF-HFP)) can also be used to form gels with [EMIM][TFSA] ILs. Compared with PS-PMMA-PS gel, their capacitance values decrease with increasing frequency. The results (Fig. 3b) show that the capacitance value of P(VDF-HFP) gel is approximately 1 μF lower than that of SMS gel at a low frequency (10 Hz), however it is slightly higher than that of the SMS gel at a high frequency (100 kHz)[56]. This proves that the dielectric functions of the two EDL dielectric materials are comparable. To achieve good implantability of flexible electronic devices, biocompatibility must also be ensured for the materials

Table 1. Parameters comparison of Ionic-gel Gate Transistor.

μ_F (cm^2 V^{-1} s^{-1})	$I_{On/Off}$ ratio	SS (mV)	Vth (V)	Ionic liquid	Polymer	Channel	Method	Ref
20	10^5	158	−0.13 V	[EMI] [TFSA]	P(VDF-HFP)	In$_2$O$_3$	Cut and stick	[55]
20	10^4	110	−0.2 V	[EMIM] [TFSI]	PS-PMMA-PS	PQT-12	Cut and stick	[53]
20	10^5	270	−0.5 V	[EMIM] [TFSI]	PS-PEO-PS	PQT-12	Cut and stick	[53]
20	10^5	nr	0.12 V	Proton	Wheat flour	IZO	Drop	[67]
2	10^5	670	0 V	[EMIM][TFSI]	P(VDF-HFP)	IWO	Cut and stick	[25]
nr	10^5	nr	12 V	[BMIM][PF$_6$]	PS-PEO-PS	P3HT	Cut and stick	[57]
20	10^5	280	−0.7 V	[BMIM][PF$_6$]	PS-PMMA-PS	P3HT	Cut and stick	[53]
2.06	10^5	nr	−1 V	[EMI] [TFSI]	PS-PMMA-PS	ZnO	Spin-coating	[54]
nr	10^5	73	−0.8 V	[EMIM][TFSI]	P(VDF-HFP)	P3HT	EHD	[60]
nr	10^6	nr	−1 V	[P$_{14}$] [TFSI]	SOS-N$_3$	P3HT	Photo-pattern	[132]
7.8	10^5	135	1 V	Proton	Chitosan	ZnO	Spin-coating	[133]
11	10^5	90–110	0.65 V	[EMIM][TFSI]	PS−PMMA	SWCNT	Printing	[134]
1.8	10^2	nr	1.2 V	[EMIM][TFSI]	PS-PMMA-PS	WO$_3$	Cut and stick	[135]
nr	10^5	nr	0.5 V	[EMI] [TFSI]	SEAS-N$_3$	ZnO	Screen-printed	[122]
nr	10^2	nr	−0.2 V	[EMIM][TFSI]	P(VDF-HFP)	CuSCN	Cut and stick	[136]
2.3	10^5	nr	0 V	[EMI][TFSA]	P(VDF-HFP)	P3HT	Cut and stick	[56]

used in co-polymers. Therefore, some researchers use biocompatible materials, such as polysaccharides[59], chitosan[63,64], and proteins[65] instead of cross-linked polymers[66]. As mentioned before, Kim et al. proposed an ionic gel made of Lewandan polysaccharide and choline-based water-soluble IL cast by a simple solution method (shown in Fig. 3c). This dielectric has the characteristics of good biocompatibility, biodegradability, high transparency, free stranding, and solid state[59]. Besides, Yang et al. dissolved wheat flour and acetic acid in water and prepared a wheat flour electrolyte membrane by a drop-casting method. The resulting IZO-based thin-film transistor exhibited a switching ratio of 10^5, and have excellent saturation mobility (15 cm^2 V^{-1} s^{-1}). Accordingly, they realized the simulation of synaptic functions, such as excitatory postsynaptic current (EPSC) and paired-pulse facilitation (PPF)[67].

Furthermore, some mixed copolymer has more application compatibility and enables realize photo-crosslinking, specific recognition, acid-base resistance, hydrophilic, and hydrophobic control, etc. by controlling the internal components. A UV-curable ionic gel can easily realize the preparation of ultra-tiny IGTs[68]. In addition, Liu et al. also prepared a fully stretchable polarized transistor by controlling the PFPE content in the PFPE-DMA gate dielectric layer. They demonstrated a skin-like display that is formed by integrating stretchable TFT array and stretchable organic light-emitting electrochemical cells (OLECs) (Fig. 3d)[69]. Through the preparation method compatible with traditional MEMS technology, the application of IGTs in fields, like health monitoring and logic operation, will be further expanded.

SENSING APPLICATIONS OF IONIC-GATE TRANSISTORS (IGTS)

In 1970, Bergveld et al. discovered that after removing the gate of the FET and immersing it in a liquid, the ions in the insulating layer would affect the conductivity of the channel layer. Therefore, the original IGT was used as a sensitive ion sensor and used in physiological detection. Nowadays, IGT has become a hot research topic among multidisciplinary areas including electronics, neuromorphology, biology, and engineering. Various exciting applications of IGT have been developed continuously. For example, due to the excellent light transmittance of ionic gels, IGT also has broad application prospects in the field of optics[10]. The properties of IGT, such as stable structure, stable chemical properties, and

stretchability, have attracted much attention in the field of wearable electronics. Not only can it be used as a mechanical sensor to sense pressure, but it can also be used as a proximity sensor or smart sensor in sensing, thereby improving signal processing efficiency and reducing system power consumption.

In the field of optoelectronics, phototransistors and optical modulators take full advantage of IGTs[70]. Phototransistors that receive optical signals and convert them into electrical signals can detect light in various bands, therefore, enabling applications of night vision, three-dimensional object recognition, health monitoring, and optical communications[71,72]. Owing to their three-terminal configurations, phototransistors can effectively reduce noise and amplify electrical signals. Meanwhile, ionic gel electrolytes are introduced due to its high capacitance and transparency to solve the problem of high operating voltages[73]. Thus, the ionic gel has been used to achieve low operation voltage and high carrier concentration, while the low mobility of the ions and formation of the layered effect can help realize optical modulation.

In order to obtain a strong electric field at the interface between the gate and the channel, EDLT is a promising choice, which can generate high carrier density at low pressure. Many studies have used IGTs to achieve electrical and optical multi-modal control of the channel layer, and further applied to neuromorphological research[55]. Much more interesting, Ionic-gel-based photonic devices with simple processing and high gate-capacitance, dynamically regulate the graphene chemical potential (Fermi level) (Fig. 4)[74]. The charge density is electrically tuned at the ionic gel–graphene interface, and the chemical potential of graphene is changed to control its intensity of light absorption. At 1.55 μm wavelength, the transverse-magnetic (TM) mode is increased from −10.8 dB to −8.8 dB, and the transverse electric (TE) mode is reduced from −9.0 dB to −12.1 dB. Depending on these data, the waveguide sample with an ionic-gel gate dielectric can be used as a broadband TM transmission polarizer. In addition, the optical behavior of the ion-gated modulator clearly shows hysteresis due to the slow polarization response time.

Further, a research study has recently demonstrated that photoluminescence (PL) can be reversibly tuned by EDLTs up to 1–2 orders of magnitude at a low gate voltage (Fig. 4c, d)[75]. The density of electron traps via the interaction of trap with oxygen ion at $V_g < 0$ is reduced, owing to the transverse gate-electric-field
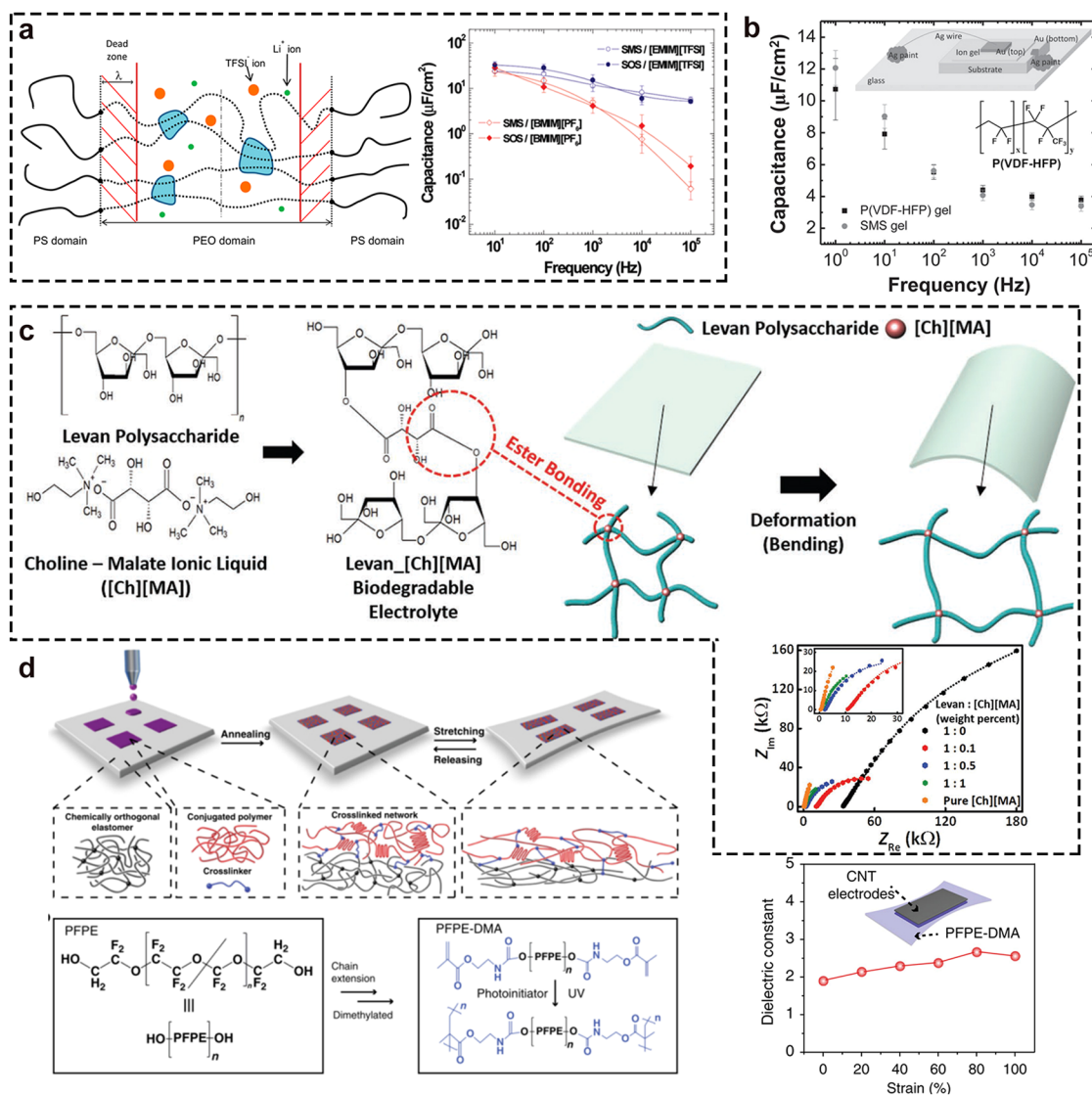
Fig. 3 Four different types of polymer materials used for an ionic-gel transistor. a SOS, a schematic diagram of the structure of a triblock (ABA) polymer. Reproduced with permission[131]. Copyright 2014, American Chemical Society. Capacitance-frequency dependence of four different ionic-gel. Reproduced with permission[53]. Copyright 2009, American Chemical Society. **b** Comparison of the frequency dependence curves of the maximum capacitance of SMS and P (VDF-HFP) materials. The inset is a schematic diagram of the molecular structure and device structure of P(VDF-HFP). Reproduced with permission[56]. Copyright 2012, Wiley-VCH. **c** The molecular structure of Lewandan, the synthetic ionic liquid based on choline and malate ions, and the chemical structure and schematic diagram of the expected synthesized LSE membrane. On the below side is the Nyquist chart of LSE. Reproduced with permission[59]. Copyright 2020, Wiley-VCH. **d** The schematic diagram shows the material design used to pattern stretchable transistors on elastomer dielectrics by inkjet printing. The figure on the right shows the dielectric constant of the PFPE-DMA film subjected to uniaxial strain. Reproduced with permission[69]. Copyright 2020, Springer Nature.

generated by ionic gels, leading to lower probabilities of non-radiative recombination and photogenerated carriers with increased mobility, and accordingly, the PL density is enhanced. The function of reversible control of perovskite luminescence can be advantageous to the potential applications of photons in perovskite materials.

Moreover, optical frequency combs are the basis of modern frequency measurement, astronomical observation, precision spectroscopy, ultrafast optics, and quantum information[76,77]. Yao et al. pioneered the application of IGTs in graphene-based tunable optical frequency combs (Fig. 4e)[78]. By coupling the ionic-gel gate-tunable light guide to the silicon nitride photonic microresonator, the second- and higher-order dispersion can be modulated by tuning the Fermi level. They have successfully demonstrated a double-layer IGT that can adjust the Fermi level of graphene to 0.45–0.65 eV, besides, the double-layer IGT is able to retain a cavity mass

coefficient of up to 10[6]. Resulting from merging single atomic layer nanoscience with ultrafast optoelectronics, this heterogeneous graphene microcavity can further enhance our understanding of dynamic frequency combs and ultrafast optoelectronics.

The FET-type pressure device is one of the basic component of electronic skin devices that achieve advanced sensing performance, including multi-parameter tracking, high sensitivity, high resolution, and low crosstalk signaling[79–82]. In an earlier study, ionic-gel-based FETs have been observed to function by inducing mobile charges in the semi-conductor channel and are utilized to fabricate pressure sensors with low power consumption and high transparency[58,83]. For example, Khademhosseini et al. demonstrate an IGT-based pressure sensor[84]. The dielectric layer is fabricated by microstructured ionic hydrogel, shown in Fig. 5a–d. As external pressure is applied to the top of the transistor, the microstructure hydrogel deforms and changes
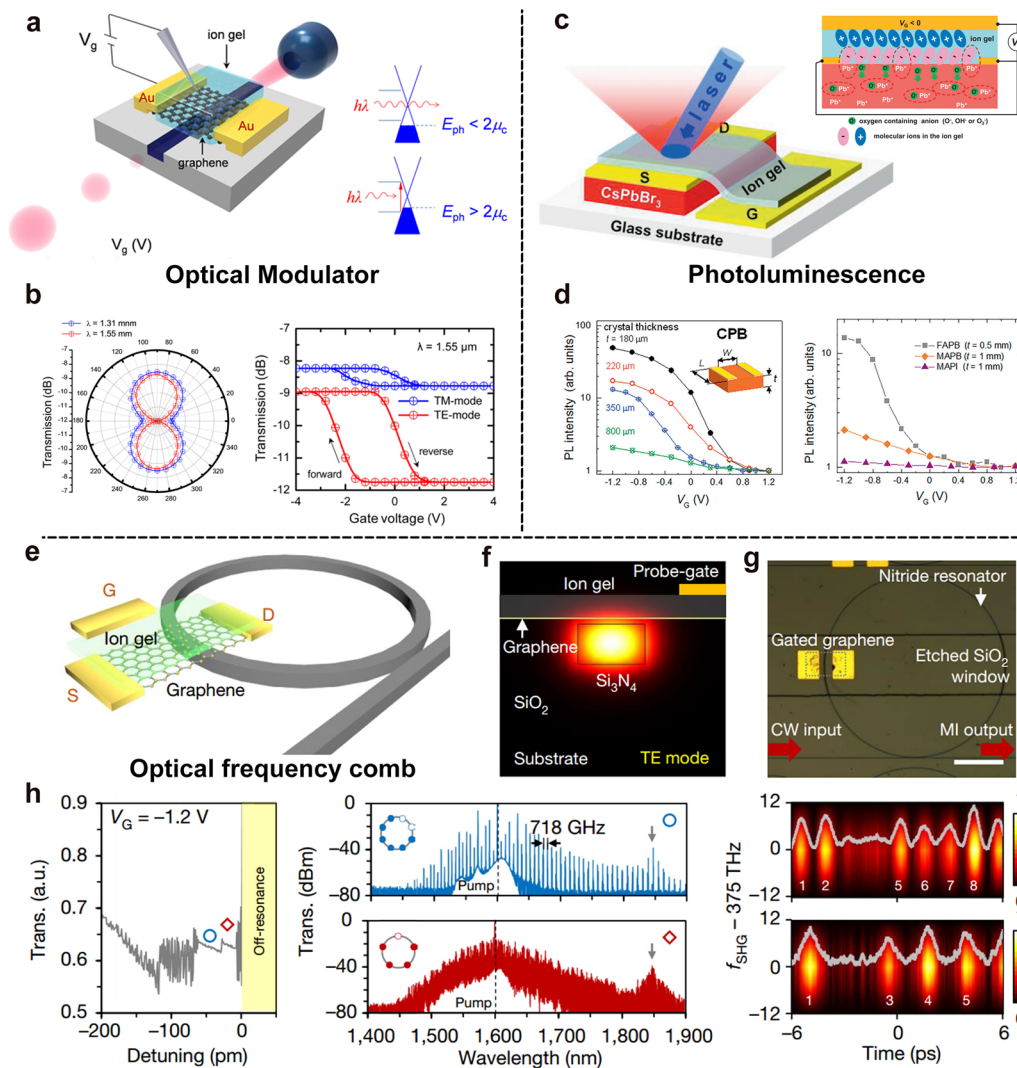
Fig. 4 Applications of phototransistor formed by ionic-gel. a Schematics of ionic-gel-integrated optical-transistor modulator. Reproduced with permission[74]. Copyright 2017, American Chemical Society. **b** The polar image measured under the presence of the ionic-gel and the optical transmission of phototransistor according to the top gate voltage at a wavelength of 1.55 μm. **c** Scheme of the IGT photoluminescence devices with a lead-halide perovskite single-crystal integrated with an ionic gel. Reproduced with permission[75]. Copyright 2019, Elsevier. **d** The relationship between V_G-induced modulation of PL intensity and the device geometry (the crystal thickness and photoexcitation area) of perovskite EDLTs. **e** Schematic architecture of the graphene-based microresonator. The gray object showed is the silicon nitride. Reproduced with permission[78]. Copyright 2018, Springer Nature. **f** Electric field distribution of the graphene–nitride heterogeneous waveguide, with a Si_3N_4 cross-section of 1.2×0.8 μm². The distance between the Si_3N_4 waveguide and the graphene layer is 100 nm. The graphene and the top-gate probe are separated by 1 μm with the interlayer ionic-gel capacitor. In this structure, transverse electric (TE) mode is applied. **g** Optical micrographs show the bus waveguide (red arrows), ring resonator, and Au/Ti metallized patterns. An etched window is designed to ensure both graphene–light interaction and reduced propagation loss. Here the graphene-covered area is marked by the gray dashed box; the etched window label refers to the whole horizontal area between the two central lines. CW continuous wave, MI modulated intensity. Scale bar, 100 μm. **h** Soliton state with crystal-like defects modulated by heterostructure transistor. The middle and right graphs are the corresponding spectral measurements and the frequency-resolved second harmonic autocorrelation graphs of soliton pulses. The gray curve here shows the real-time autocorrelation intensity curve.

the capacitance of the hydrogel/gate interface, as a result, affecting the number of ions in the channel. Due to the outstanding amplify capability of the organic electrochemistry transistor (OECT), the pressure sensor can detect pressure as low as 20 Pa in this manner. Furthermore, the IGT operates at a lower voltage (0–1 V) due to the high capacitance of the EDL effect, and the entire power consume of sensing device used is only 10–1000 μW. Based on these two advantages, ionic gel-based pressure sensors are also competitive in wearable and implantable sensor applications.

Cho et al. proposed a structure for the fabrication of pressure sensor matrices with a simple process and excellent performance[83]. The ionic-gel connects the drain and the gate, and the ionic-gel gate capacitance under the double capacitance effect is large (7.9 μF cm⁻²), which ensures that the graphene FET works at a low gate voltage of less than 2 V. Between the source and drain electrodes, the interdigitated electrode at the bottom is in contact with the graphene backplate under external pressure, resulting in a change in resistance (shown in Fig. 5e). It exhibited high-pressure sensitivity (0.12 kPa⁻¹) and outstanding mechanical durability (more than 2500 cycles). With the help of this structure, the fabrication of common-gate array devices can be easily realized. The pressures on the 4×4 GFET matrices can be mapped spatially (Fig. 5f).

However, the use of transistors as direct pressure sensors is limited by structural design difficulties and poor stability,
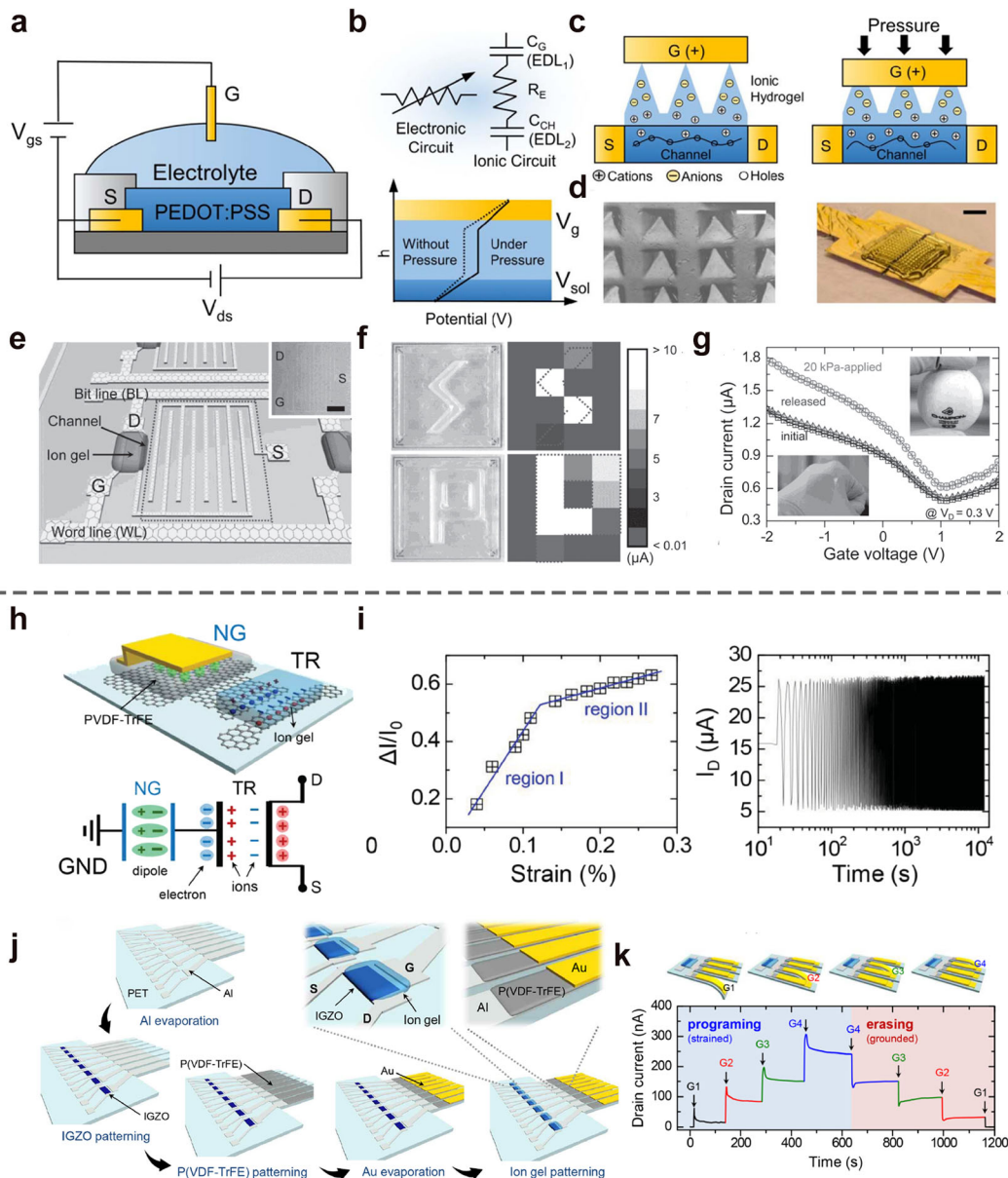
Fig. 5 Piezo electronics sensor made of ionic-gel transistor. a Schematic diagram of the device structure of an OECT. **b** quivalent circuits in an OECT and schematic diagram of the proposed microstructured hydrogel-gated OECT iontronic pressure sensor. The deformation of the hydrogel determines the number of ions delivered into the channel. **c)** V_g and V_{sol} change after application of external pressure on the gate electrode. **d** SEM image of gelatin methacryloyl (GelMA) hydrogel with pyramidical microstructures on the surface; Lower picture is a real optical image of the OECT iontronic pressure sensor. Reproduced with permission[84]. Copyright 2021, IEEE. **e** Schematic diagram of a GFET pressure sensor fabricated with interdigitated source electrodes. **f** Spatial pressure graph of GFET pressure sensor matrix. **g** Pressure sensing characteristics of GFET pressure sensor mounted on PDMS rubber substrate. The illustration shows the GFET matrix making angular contact with human hands or table tennis. Reproduced with permission[83]. Copyright 2014, Wiley-VCH. **h** Mechanism of GT strain sensing based on piezoelectric potential gating. **i** Sensitivity and stability characteristics of piezoelectric gated GT strain sensor. Reproduced with permission[58]. Copyright 2015, Wiley-VCH. **g** Process for manufacturing multi-level non-volatile memory array for piezoelectric potential programming. **k** Real-time programming and erasing steps applied to piezoelectric potential programming memory. Reproduced with permission[93]. Copyright 2016, American Chemical Society.

prompting researchers to turn to other methods. The piezoelectric effect is defined as the electric polarization of the piezoelectric material that originates from materials that lack inversion symmetry, caused by the action of external mechanical forces; piezoelectric materials convert random mechanical energy into electric energy (piezopotential power)[85,86]. The piezotronic transistor, utilizing inner-crystal piezopotential to harvests biochemical and biomechanical energy[87,88], while achieving self-powered active digital data processing capacities, such as pressure arrays with high resolution and human-machine interaction[89,90].

Ionic-gel electrolyte materials are extensively applied in piezotronic transistors owing to their large capacitance that enables low-voltage transistor operation[91,92]. The long-range polarization characteristics of ions in the ionic gel allow the placement of the gate electrode and channel to be coplanar. Sun et al.[58] described a piezopotential-powered active strain sensor matrix array combining piezoelectric nanogenerators (PENGs) and coplanar-gate graphene transistors based on P(VDF-TrFE), as shown in Fig. 5h. The output pressure sensor signal is maintained at the corresponding value based on the applied strain. The ionic-gel

dielectrics can effectively couple the piezoelectric potential to the graphene channel, thereby maintaining the output sensor signal at the corresponding stress value. As a result, excellent sensitivity (GF = 389), ultra-high detection limit (0.008%), and high mechanical durability (> 3000 cycles) are obtained (Fig. 5i). They further developed a piezopotential-programmed non-volatile memory array by integrating ionic-gel-gated FETs and PENGs[93]. The storage device is programmed by applying external pressure to the PENG, and by grounding the top electrode of the PENG. In contrast, it is easy to flash the stored data by grounding the upper electrode of the PENG (Fig. 5g). Under various external bending strains, multi-level data storage of more than 3 orders of magnitude is achieved with a good memory efficiency, including a high programming/erasing current ratio (> 10^3), 2-bit multi-level data storage (over 4 levels), efficiency reliability over 100 cycles, and reliable data retention over 3000 s.

With the advent of the Internet of Things (IoTs), non-invasive measurements and real-time health monitoring have become increasingly important in modern medicine, particularly to address the urgent needs of the aging population[40]. In the process of medical monitoring and diagnosis, equipment with high-quality signals and long-term stability is essential[94]. In addition, soft devices with good physiological comfort and biological compatibility can effectively minimize the harm to the human body and discomfort of wearing[2,95–99]. IGTs have the key advantages of low threshold voltages, high amplification, and biocompatibility[100,101] that ensure an accurate diagnosis of physical illness. Therefore, IGTs that are intrinsically stretchable, adequately meet the needs of physiological monitoring.

In conventional methods, medical monitoring and diagnosis mainly rely on physiological signals (blood pressure, heart rate, and respiratory rate) and the real-time concentration of biochemical molecules (Na^+, K^+, glucose). Transistors can achieve an effective amplification of these data and thereby effectively improve the sensitivity of medical sensors. For example, Someya et al.[102] fabricated a biocompatible electrode by integrating a gelatinous composite into transistor amplifiers to realize a direct detection of pericardial electrocardiography (Fig. 6a). One-pot fabrication of a conductive gel that is responsive to glucose without enzyme, is integrated into OECTs to detect the patient's glucose level clinically[103]. Alcohol dehydrogenase (ADH) and its nicotinamide adenine dinucleotide (NAD^+) cofactor are readily immobilized on the OECT to detect ethanol in the range of 0.01 % to 0.2 % blood alcohol content (Fig. 6b)[104].

Although gel-based transistors have realized various applications in the medical field, there is still a lot of scope for improvement. The first problem that needs to be solved in this field is the requirement of the high-level accuracy of physiological signals to provide an accurate diagnosis, and this is dependent on the SNR (signal-to-noise ratio)[105,106]. To obtain a high SNR, a preamplifier may be integrated in close proximity to the sensing electrode to reduce the influence of the wiring noise, thereby realizing active elements with local signal amplifications[102,107]. The structure of OECT without the gate dielectric layer makes direct electrolytic operation possible, allowing the conversion amplifier to be directly loaded at the location of the target, thereby largely reducing the ratio of noise. Someya et al.[108] designed an OECT-based electrophysiological transducer with a high SNR (24 dB). They successfully solved the issue of the inability of transistors to operate for a long time due to electrolyte drying, by integrating an ultra-thin OECT with a nonvolatile gel electrolyte, as shown in Fig. 6c. OECT made of thin gels can adhere well to the skin and effectively monitor the heart signal. It demonstrated stable performance during long-term continuous monitoring (for example, within 3 h) and multiple reuses in tests, lasting more than a week (Fig. 6d).

Another major achievement is the technological advances in flexible and biocompatible materials that not only allow patients to have a better wearing experience, but also facilitates real-time monitoring. Unlike previous studies that have fabricated ultra-thin inorganic semi-conductors or have designed "wavy" structures to achieve flexibility[109,110], intrinsically stretchable conductive polymers have become a growing trend. Kim et al.[59] synthesized biocompatible, biodegradable, highly transparent, free-standing, and solid-state electrolytes consisting of levan polysaccharide and choline-based water-soluble IL (as shown in Fig. 6e). Levan polysaccharides function as free-standing and solid-state polymeric matrices that are translucent, versatile, and water-soluble, while choline-type water-soluble IL reacts with malic acid, utilizing choline as the cation and malic acid as the anion[108]. Biodegradable electrolyte-based organic transistors exhibit satisfactory performance, such as low operating voltage ($V_{ds} = -1.0$ V and $V_{gs} = -2.0$ V), good stability, and high on/off ratio (over 10^3). Organic transistors were incorporated with bio-integrated instruments, such as electrocardiogram (ECG) recordings on human skin and rat heart with a better signal-to-noise ratio (shown in Fig. 6f).

A thread-based transistor (TBT) realized by electrolyte gating of semiconducting carbon nanotube networks on linen threads was proposed by Sameer et al. The thread has an interchangeable module to fit the biological tissue required, can be minimally invasive (for example, sutures), and enables the provision of three-dimensional tissues or organs with a natural interface[111]. The electrolyte is composed of colloidally scattered nanoparticles of silica and IL gel (a form of an ionic gel) that enables CNT transistors to be electrostatically gated. To achieve a multiplexed diagnostic system based on complete threads, they linked TBTs with thread-based electrochemical sensors (TBEs). As seen in Fig. 6g, completely threaded platforms are thin, extremely durable, and compatible, allowing them to be worn directly on the skin without any silicone substrate or without using a skin needle. As mentioned above, most ionic gels consisting of polymers and ILs are not proven to be biocompatible and biodegradable, and some of them are even toxic to humans. Therefore, it is necessary to apply natural biomaterials such as cellulose or hydrogels with non-toxic synthesis procedures.

NEUROMORPHOLOGY APPLICATIONS OF IONIC-GATE TRANSISTORS (IGTS)

Another emerging application of IGT is neuromorphic devices, particularly synaptic transistors. In order to simulate the human brain, much efforts have been invested in the ability of parallel processing of data and weight modulation through algorithms and software on the existing computer hardware[112,113]. However, the human brain performs better than traditional computers while processing real-time sensory data such as images, videos, sounds, and navigation. In addition, compared with the high energy consumption of supercomputers, low energy consumption is also a major advantage of the biological brain[114]. Synapse transistor is imitated as a synapse, where two neurons are connected functionally, and they are also the key parts of signal transmission, as shown in Fig. 7a. The human brain is a complex network composed of nearly 10^{11} neurons and 10^{15} synapses that are highly interconnected, massively parallel, and structurally variable[115]. Synaptic plasticity, as a functional feature of nerve cell interconnection, gives biology the ability to learn and remember. The appearance of hysteresis of EDLT devices limits its switching speed, and is not suitable as a conventional transistor, but is more suitable as a functional device that mimics synaptic transmission. The bionic simulation of brain nerve structure provides many feasible research scopes. Based on the phenomena of dendrites receiving multi-synaptic signals, Wan et al. controlled the information transmission of neuromorphic transistors through multiple in-plane gates[116] (Fig. 7b). Owing to the different distances between the source and drain electrodes and the multiple gates, the spatial position of each gate on the plane is defined by different coordinates. Obviously, the spatial coordinate
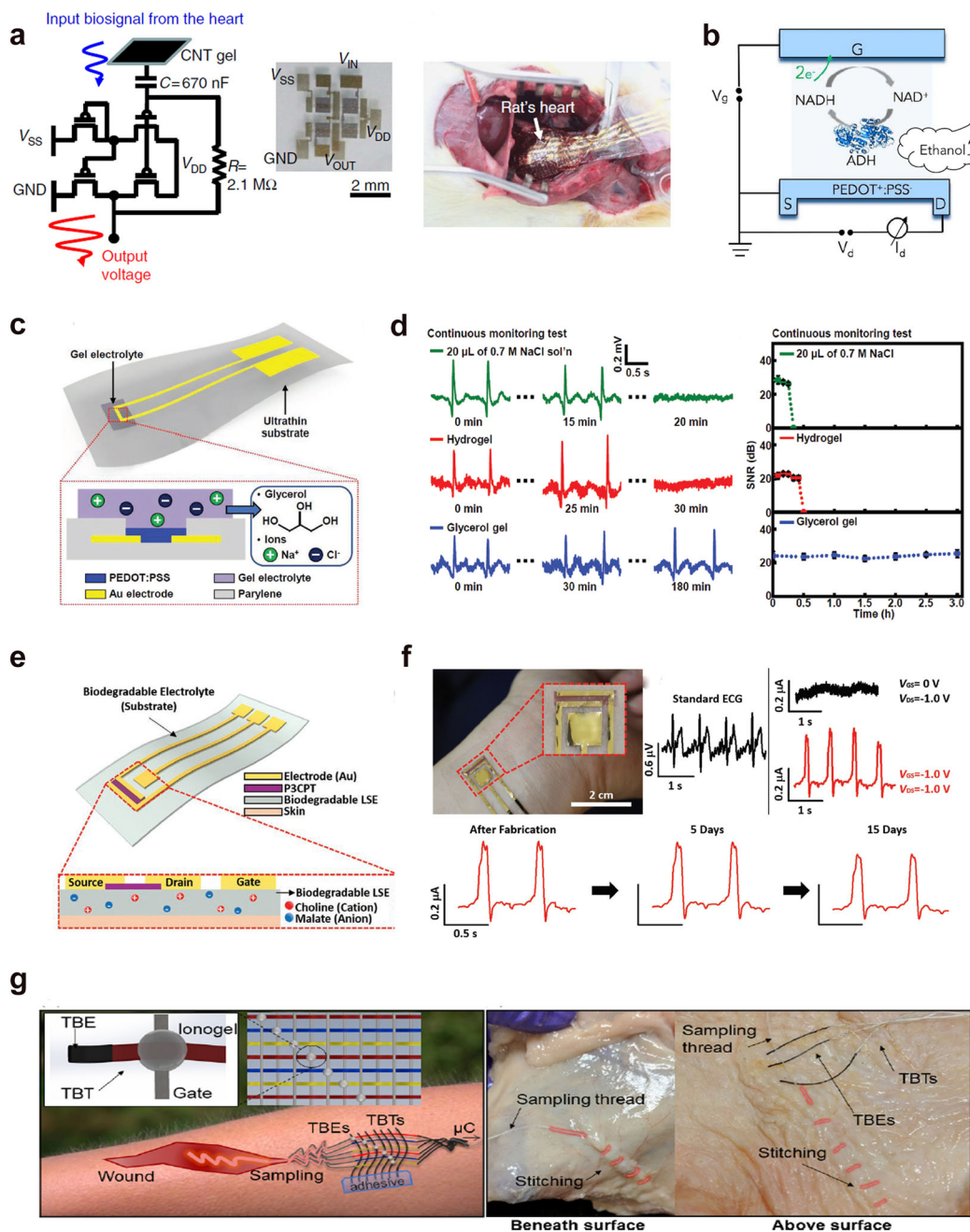
Fig. 6 Bio-sensors made of ionic-gel transistor. a Circuit diagram of a unit of an organic amplifier with a conductive gel for an in vivo electrocardiograph and Pictures of an ultra-flexible circuit on a rat's heart. Reproduced with permission[102]. Copyright 2016, Springer Nature. **b** Enzymatic reaction of ethanol and ADH in an electrolyte. Reproduced with permission[104]. Copyright 2016, Springer Nature. **c** Schematic diagram of OECT in a nonvolatile gel electrolyte containing glycerol and ions. **d** OECT-based sensors measured ECG data at different electrolytes (0.7 m NaCl, hydrogels, and glycerin gels) Reproduced with permission[108]. Copyright 2019, Wiley-VCH. **e** Schematic of a biodegradable organic transistor. **f** Standard equipment and biodegradable organic transistors record the ECG signals from the human skin. Reproduced with permission[59]. Copyright 2020, Wiley-VCH. **g** Schematic diagram of a thread-based integrated transistor system for advanced sensing of bio-related ions. Reproduced with permission[40]. Copyright 2019, American Chemical Society.

of the gate closer to the channel layer contributes more significantly to the weight of the transistor. The mapping of distance and EPSC contribution is shown in Fig. 7c. They present EPSC current diagrams for different stimulation directions and the I/O relationship between the rate coding scheme and neurons in different directions. They further verified the influence of stimuli directivity on multi-gate neuromorphic transistors (Fig. 7d).

Real-time control can be achieved through a programmable circuit design. John et al. also utilized P(VDF-HFP) and [EMIM][TFSI]

as the dielectric materials to prepare neuromorphic memtransistor elements[25]. By defining different gate voltages as different harmful inputs, they successfully used IGTs to simulate the modulation of the salient weight of pain receptors. Similar to bio-nociceptors, the satellite threshold adjusting receptors (STARs) can adjust the transfer characteristic curve of the device according to the intensity of the harmful stimulus (V_{gs}) to make it more sensitive and avoid repeated damage. When V_{gs} is higher than the threshold voltage and the duration increases, significant transistor
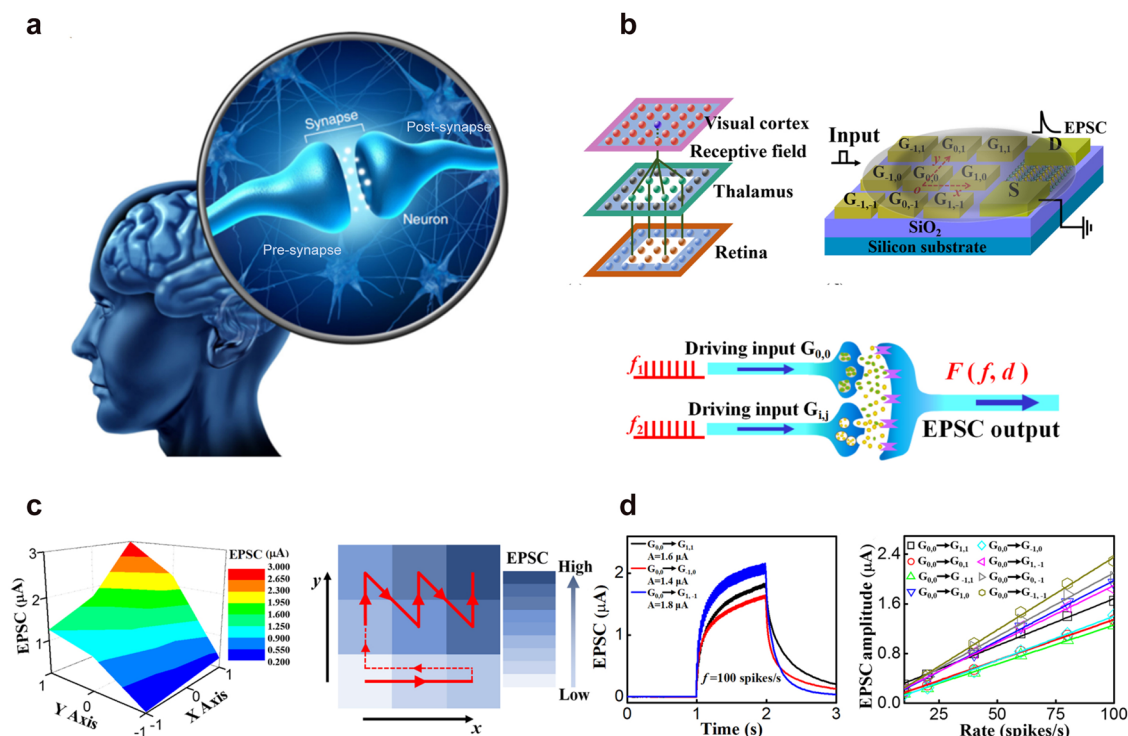
Fig. 7 The scheme and functions of multi-synapse. a Schematic illustration of a Biological network. Reproduced with permission[25]. Copyright 2020, Springer Nature. **b** Schematic picture of the visual system and 2D MoS_2 neuromorphic transistor with a grid of 3×3 coplanar-gate arrays. Reproduced with permission[116]. Copyright 2018, American Chemical Society. **c, d** 2D EPSCs surface summarized as a function of spatial coordinate, and each gate has a different coordinate. EPSC responses driven by dual spike inputs and its different orientation relationships.

drift occurs, as shown in Fig. 8a–f. After a period of time or application of the recovery voltage, the threshold characteristic of IGT can be restored to its original level, as shown in Fig. 8e. The robot can change its sensitivity after receiving harmful stimuli and can realize self-healing and functional recovery after being damaged. The decentralized intelligence they proposed is different from traditional centralized intelligence and is more suitable for the requirements of future robot intelligence in terms of power consumption and application prospects.

Owing to the inherent flexibility of ionic gels, some flexible neuromorphic transistors have also been reported. Shim et al. fabricated rubber-like synaptic transistors using full rubbery elastomeric materials[26]. Based on the all-rubber materials, this rubber synaptic transistor has realized synaptic behaviors such as pair-pulse facilitation (PPF), synaptic filtering, and current enhancement after excitation. They studied the excitatory postsynaptic current drops from 82.21 μA to 77.15, 44.54, and 41.8 μA without damage, when the rubber synaptic transistor was stretched by 10% and 30% to 50%, as shown in Fig. 8h. With an increase in the pulse width at the frequency of 5 Hz, the synaptic device exhibits the functions of sensory memory, short-term memory, and long-term memory (Fig. 8i). Figure 8j shows that the flexible synaptic transistor is excited at 20 Hz, and the excitatory postsynaptic current response of 0% and 50% strain is significantly different. They defined the gain strength of A_{20}/A_1 and used it to measure the effect of strain. Obviously, the strength of the gain is also related to the pulse frequency, pulse width, and pulse peak value. They further used triboelectric nanogenerator as power supplies to build an integrated soft adaptive neural robot (Fig. 8k). This soft neurorobotic system receives external pressure stimuli and produces bending movements, which is suitable for the application of building humanoid robots in the future.

Many inorganic nanomaterials or organic semi-conductor materials have excellent response characteristics to light waves of different wavelengths[10,117]. Further, inspired by biological visual and nervous systems, Sun et al. demonstrated a flexible, dual-modulation, tunable synaptic FET based on ZnO nanowires as the channel, and sodium alginate as the gate[118]. IGT is combined with ZnO that has an excellent UV light response, it can also output a higher current than the normal state after multiple UV light stimulations. The optical image, transfer characteristics, and optical responses of the synaptic field-effect transistor (SFET) on a PI substrate are shown in Fig. 9b. The threshold voltage V_{th} of the SFET moves to the left under the various forces of UV radiation, demonstrating the implementation potential of the system in terms of artificial optical synapses. The light spike stimulates the transistor as the action of a positive gate voltage. A matrix of SFETs has been manufactured and verified to investigate the uses of SFETs in artificial visual systems (As shown in Fig. 9d).

IC APPLICATIONS OF IONIC-GATE TRANSISTORS (IGTS)

Much effort has been made in applying IGT to IC functions, like inverter, which is the basic function of advanced integrated circuits[119]. The most commonly used structures of inverters in recent years are two forms: single-component FET and complementary FET[120]. The single-component FET inverter is consists of one FET and a resistor. Frisbie et al. reported an EDL-FET using SMS ionic-gel as gate dielectric on a poly (ethylenenaphthalate) (PEN) substrate (Fig. 10a). They adopted whole organic material to fabricate this low-cost OFET, instead of Au. The switching V_{th} is zero, and completed within 0.5 V, shows a high gain at 7[121]. Furthermore, they used IGT to prepare a CMOS inverter with high response speed and low operating voltage. Frisbie et al used stenciling technology and traditional photolithography to prepare SEAS-N_3 ionic-gel gate dielectric layer transistors[122] (Fig. 10c). The fabricated transistor is powered by a power supply sub-3 V and the inverter stage delay is close to 50 μs. More importantly, they
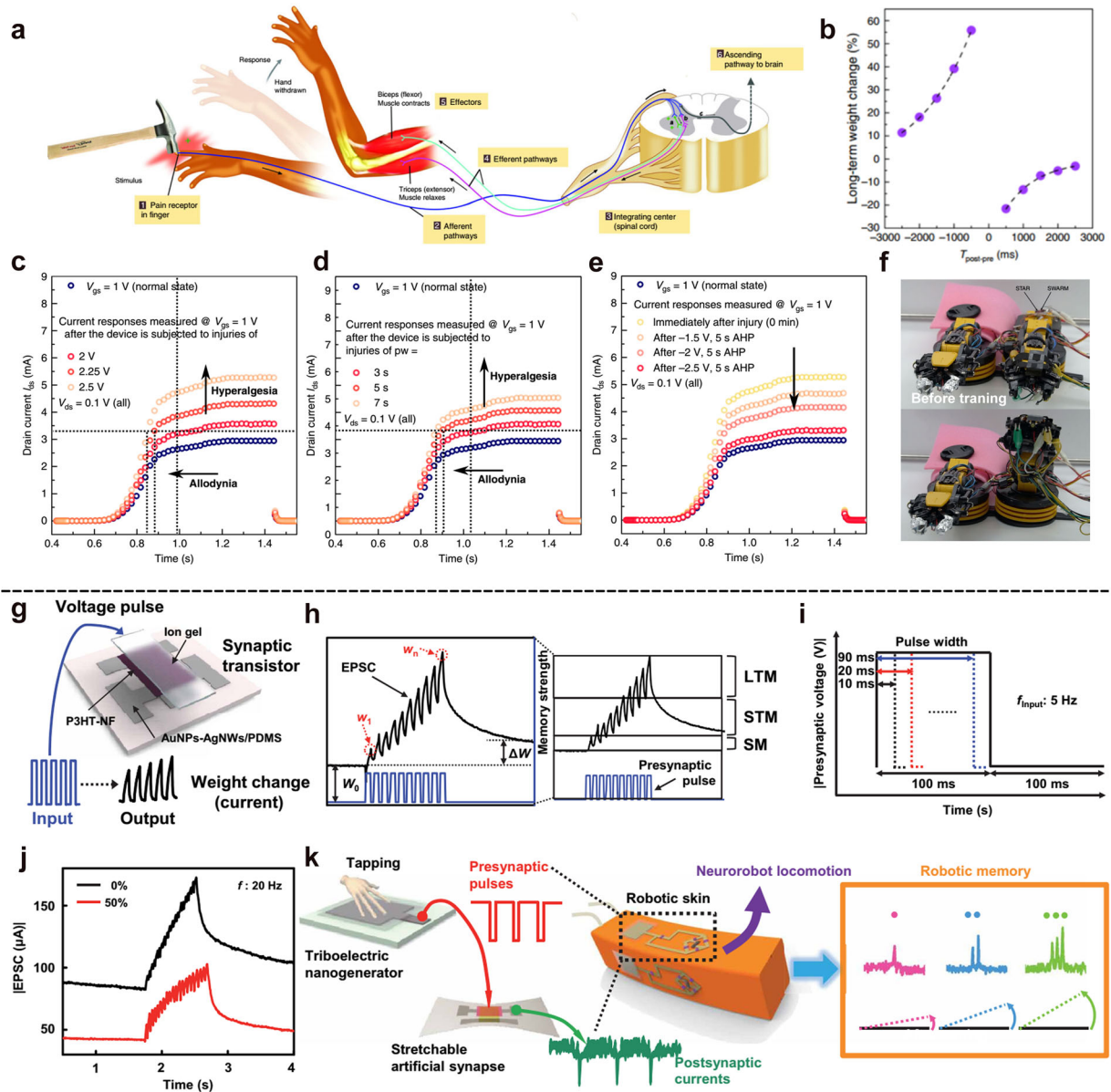
Fig. 8 The function of artificial synapse realized by IGT. a The working principle of biological nociceptors and their central nervous control. Reproduced with permission[25]. Copyright 2020, Springer Nature. **b** The weight change in SWARM follows the anti-Hebbian rule. **c–e** The low-amplitude voltage $V_{gs} = 1$ V indicates the normal state, and the high-amplitude voltage indicates damage and can cause sensitive reactions. **f** Sensorimotor platform capable of detecting and associating noxious stimuli. **g** Scheme diagram of the all flexible ionic-gel gated transistor. Reproduced with permission[26]. Copyright 2019, Elsevier. **h** Scheme of the SM, STM, and LTM. **I** Schematic diagram of pulse width adjustment at 5 Hz. **j** Measured EPSCs of IGTs in response to presynaptic pulses at 20 Hz, under the strain with 0% and 50%. **k** Schematic illustration of the soft neurorobotics and its programmed operation based on robotic memory decoded signals.

claim that through further optimization, especially in terms of the ion conductivity of gel, the stage delay can be shortened to the order of 1 µs. There is no doubt that this will greatly expand the potential applications of ionic-gel transistor circuits.

In addition to the functional devices of traditional integrated circuits such as inverters, ionic-gel transistors can also be used as organic memory devices due to their reverse ion characteristics[123–125]. Koo et al. reported nonvolatile transistor memories (NvTMs) devices that depend on the formation of EDL[126] (Shown in Fig. 10e). The IGZO film pattern was prepared by spin coating and UV curing. The transfer characteristics of Au nanoparticles device are shown in Fig. 10f. They separately analyzed the induction of the gate on the IGZO surface through the EDL effect under the write voltage V_{prog} and the erase voltage V_{era}. Colloidal gold nanoparticles are used at the interface of

IGZO, and the organic amine ligand molecules therein serve as the nano-scale tunneling dielectric of the gold nanoparticle core and the IGZO channel, which are not present in the evaporated gold nanoparticles. The tunneling dielectric delays the charge transfer between the Au nanoparticles and IGZO channel, and has a better retention effect on the programming/erasing signal. The memory window obtained when the program/erase voltage is 9 V, which is summarized in Fig. 10g as a function of the colloidal dispersion concentration to form the gold nanoparticle layer. It is verified that an increase in the coverage area of gold nanoparticles on IGZO is beneficial to storing more charges. More importantly, the preservation characteristics of the memory are improved relative to the nanoparticles prepared by thermal evaporation due to the position of the insulating organic ligand inserted between the IGZO channel
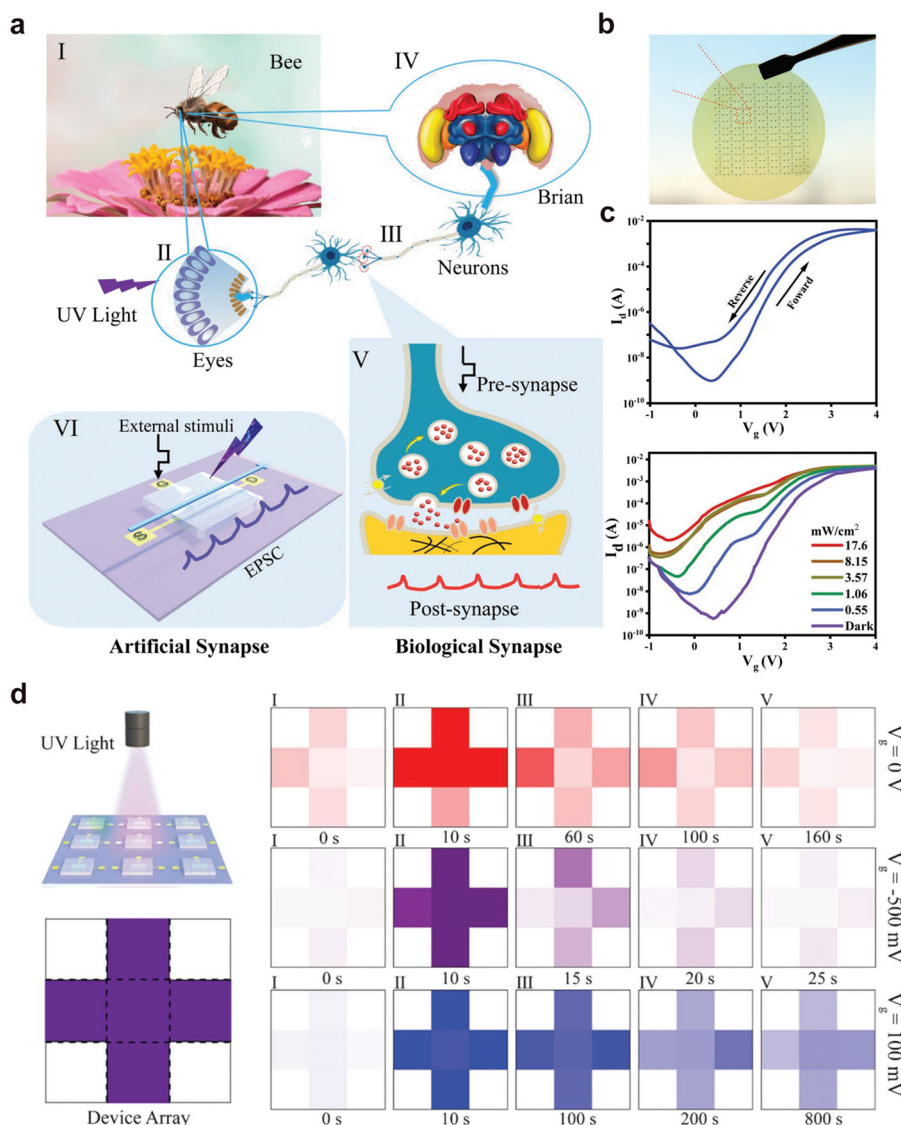
Fig. 9 The scheme and functions of a visual synapse. a Schematic diagram of device structure and bionic function. Reproduced with permission[118]. Copyright 2020, Wiley-VCH. **b** Optical photo of ZnO/SA-based SFET. **c** Electrical characteristics of the bioinspired flexible ZnO/SA-based SFET. **d** Artificial visual memory systems based on SFETs.

and the gold nanoparticle sheet. Figure 10h shows the retention characteristics of the programming and erasing signals of the IGZO nonvolatile memory prepared with colloidal gold nanoparticles (5 mg ml^{-1}). Ion-gel gated IGZO NvTM with multiple programming/ erase functions showed stable transfer characteristics in a series of cycling tests (Fig. 10i). Obviously, the drive storage device with the participation of electrolyte has a different working mode and control ability from the previous device.

CONCLUSION

We have reviewed the advances in the realization of the emerging IGTs technology. As mentioned before, the carriers induced by the large EDL-capacitance enable IGTs to be driven at much lower voltages than traditional electronic transistors, which has shown the potential contribution of IGTs in addressing energy security challenges. However, there are un-matched challenges for the processing and preparation of the ionic-gel layers for mass-scale industrialization. Spin coating, printing, and other methods have the problem of contaminating the semi-conductor layer material of the transistor, while the transfer methods generally

have low processing accuracy, and the task load is indeed heavy when dealing with high-precision systems. Merging various technologies (R2R combination transfer), maybe more suitable for rapid and low-cost preparation and application of high-precision IGTs, however further research is needed in terms of material adhesion treatment and precision control.

The good compatibility of ionic-gel materials with organic FETs further improves the shortcomings of flexible electronic technology in terms of dielectric materials. The integration of IGTs with portable power can serve a wide range of IoTs applications such as health monitoring and industrial sensing. In addition, integrated neuromorphic transistors can also provide technical support for artificial intelligence and soft robotics. Although the development of neuromorphic devices has attracted much attention, current progress is still limited to a few nerve or synaptic devices, and the functions they realize are all around the basic biological nerve functions. In addition, the energy consumption is much lower than traditional transistors, but still higher than the biological level. Finally, the multi-input neuromorphic transistor provides an alternative model for simulating the multiple connections of biological nerves, the weight modulation between multiple gates
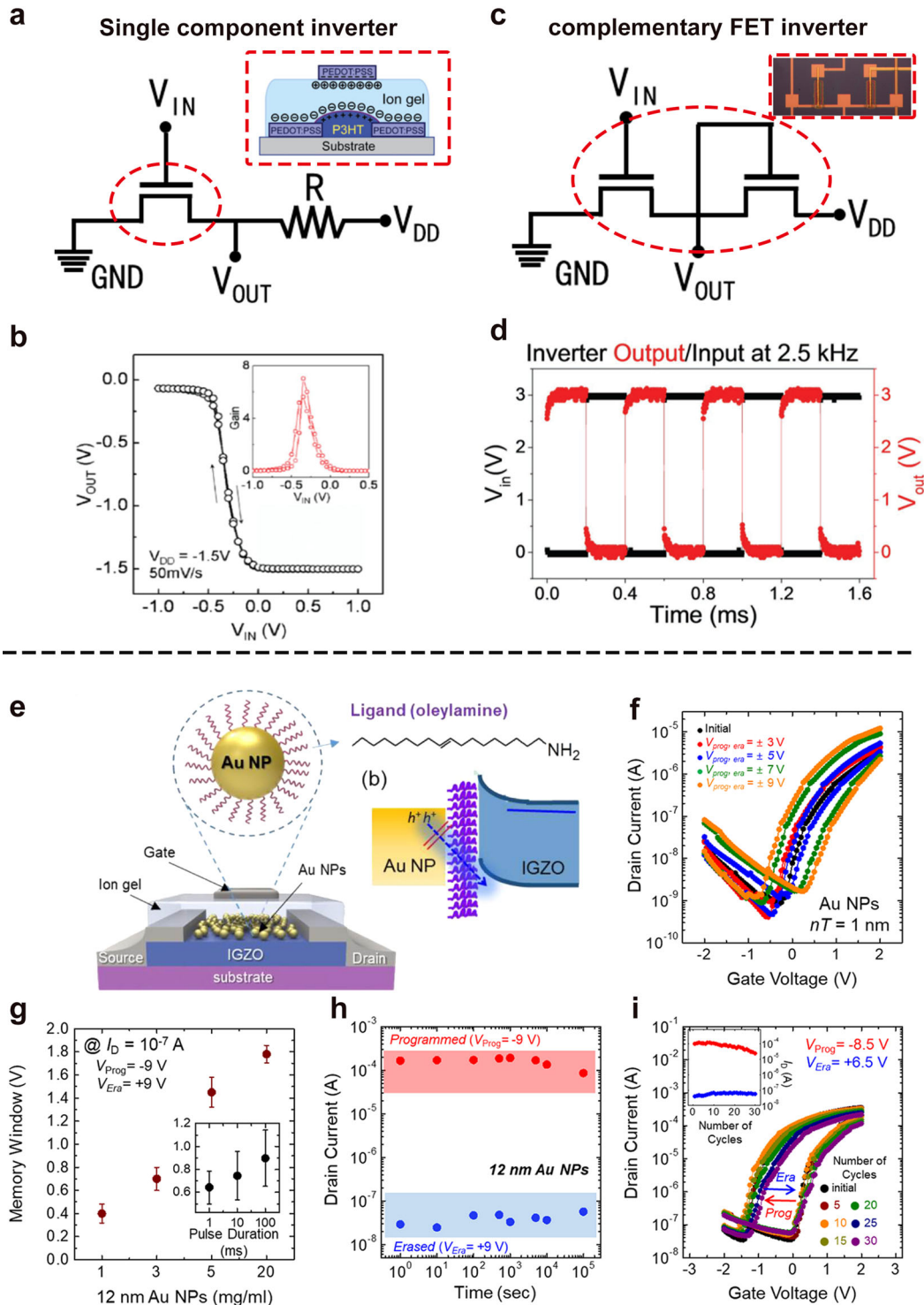
Fig. 10 Integrated circuit functions formed by ion-gel-gated transistor. a The circuit diagram of a Single-component inverter. Reproduced with permission[121]. Copyright 2010, Wiley-VCH. The inset is a scheme of an all-printed ion-gel-gated P3HT transistor with PEDOT: PSS electrodes. **b** Characteristics of a single-component inverter. **c** The circuit scheme of the complementary inverter. The upper inset shows the optical image of this complementary inverter. **d** The dynamic performance of the complementary inverter. **e** Schematic cross-section of the memory device with colloidal Au NPs with ligands. The chemical structure of the ligand molecule, oleylamine. **f** Transfer characteristics for an ionic-gel-gated IGZO NvTM containing Au NPs that were applied with different V_{prog} and V_{era}. **g** Summary of the voltage drift in the transfer characteristics of devices prepared from colloidal gold dispersions of different concentrations at $\pm 9\,V$ program/erase voltages. **h** Retention characteristics of the programmed and erased signals for an ionic-gel-gated IGZO NvTM. **i** A series of transfer characteristic curves of ionic-gel gated IGZO NvTM with multiple application/erase operations. Reproduced with permission[126]. Copyright 2018, American Chemical Society.

is also an important area for further research. To summarize, whether it is the application of the ultra-high electric field facilitated by the EDL characteristics in low-dimensional systems or the realization of biological neural networks through neuro-morphic devices, its impact on scientific research and practical applications is subversive.

REFERENCES

1. Miranti, R. et al. Exclusive electron transport in Core@Shell PbTe@PbS colloidal semiconductor nanocrystal assemblies. *ACS Nano* **14**, 3242–3250 (2020).
2. Someya, T., Bao, Z. & Malliaras, G. G. The rise of plastic bioelectronics. *Nature* **540**, 379–385 (2016).
3. Howard, I. A. et al. Coated and printed perovskites for photovoltaic applications. *Adv. Mater.* **31**, e1806702 (2019).
4. Park, M. H. et al. Ferroelectricity and antiferroelectricity of doped thin HfO_2-based films. *Adv. Mater.* **27**, 1811–1831 (2015).
5. Liao, L. et al. High-speed graphene transistors with a self-aligned nanowire gate. *Nature* **467**, 305–308 (2010).
6. Kim, S. et al. Realization of a high mobility dual-gated graphene field-effect transistor with Al_2O_3 dielectric. *Appl. Phys. Lett.* **94**, 062107 (2009).
7. Fujimoto, T. & Awaga, K. Electric-double-layer field-effect transistors with ionic liquids. *Phys. Chem. Chem. Phys.* **15**, 8983–9006 (2013).
8. Leighton, C. Electrolyte-based ionic control of functional oxides. *Nat. Mater.* **18**, 13–18 (2019).
9. Deml, A. M. et al. Progress toward a solid-state ionic field effect transistor. *J. Appl. Phys.* **111**, 074511 (2012).
10. Kang, M. S. et al. High carrier densities achieved at low voltages in ambipolar PbSe nanocrystal thin-film transistors. *Nano Lett.* **9**, 3848–3852 (2009).
11. Bisri, S. Z. et al. Endeavor of iontronics: from fundamentals to applications of ion-controlled electronics. *Adv. Mater.* **29**, 1607054 (2017).
12. Ha, M. J. et al. Printed, Sub-3V digital circuits on plastic from aqueous carbon nanotube inks. *ACS Nano* **4**, 4388–4395 (2010).
13. Lee, S. K. et al. Stretchable graphene transistors with printed dielectrics and gate electrodes. *Nano Lett.* **11**, 4642–4646 (2011).
14. Guo, J., Jiang, J. & Yang, B. Low-voltage electric-double-layer MoS_2 transistor gated via water solution. *Solid-State Electron.* **150**, 8–15 (2018).
15. Minamiki, T. et al. An electrolyte-gated polythiophene transistor for the detection of biogenic amines in water. *Chem. Commun.* **54**, 6907–6910 (2018).
16. Picca, R. A. et al. A study on the stability of water-gated organic field-effect-transistors based on a commercial p-type polymer. *Front. Chem.* **7**, 667 (2019).
17. Yuan, H. et al. High-density carrier accumulation in ZnO field-effect transistors gated by electric double layers of ionic liquids. *Adv. Funct. Mater.* **19**, 1046–1053 (2009).
18. Lieb, J. et al. Ionic-liquid gating of InAs nanowire-based field-effect transistors. *Adv. Funct. Mater.* **29**, 1804378 (2019).
19. Rawlings, D. et al. Controlling the doping mechanism in Poly(3-hexylthiophene) thin-film transistors with polymeric ionic liquid dielectrics. *Chem. Mater.* **31**, 8820–8829 (2019).
20. Herlogsson, L. et al. Downscaling of organic field-effect transistors with a polyelectrolyte gate insulator. *Adv. Mater.* **20**, 4708–4713 (2008).
21. Larsson, O. et al. Insulator polarization mechanisms in polyelectrolyte-gated organic field-effect transistors. *Adv. Funct. Mater.* **19**, 3334–3341 (2009).
22. Zhao, D. et al. Polymer gels with tunable ionic seebeck coefficient for ultra-sensitive printed thermopiles. *Nat. Commun.* **10**, 1093 (2019).
23. Li, Y. et al. Oxide-based electrolyte-gated transistors for spatiotemporal information processing. *Adv. Mater.* **32**, e2003018 (2020).
24. Seo, D.-G. et al. Versatile neuromorphic electronics by modulating synaptic decay of single organic synaptic transistor: from artificial neural networks to neuro-prosthetics. *Nano Energy* **65**, 104035 (2019).
25. John, R. A. et al. Self healable neuromorphic memtransistor elements for decentralized sensory signal processing in robotics. *Nat. Commun.* **11**, 4030 (2020).
26. Shim, H. et al. Stretchable elastic synaptic transistors for neurologically integrated soft engineering systems. *Sci. Adv.* **5**, 4961 (2019).
27. Lenz, J. et al. Vertical, electrolyte-gated organic transistors show continuous operation in the MA cm^{-2} regime and artificial synaptic behaviour. *Nat. Nanotechnol.* **14**, 579–585 (2019).
28. Bisri, S. Z. et al. Endeavor of iontronics: from fundamentals to applications of ion-controlled electronics. *Adv. Mater.* **29**, 1607054 (2017).
29. Panzer, M. J. & Frisbie, C. D. Polymer electrolyte gate dielectric reveals finite windows of high conductivity in organic thin film transistors at high charge carrier densities. *J. Am. Chem. Soc.* **127**, 6960–6961 (2005).
30. Wilkes, J. S. & Zaworotko, M. J. Air and water stable 1-ethyl-3-methylimidazolium based ionic liquids. *J. Chem. Soc., Chem. Commun.* **13**, 965–967 (1992).
31. Susan, M. A. et al. Ion gels prepared by in situ radical polymerization of vinyl monomers in an ionic liquid and their characterization as polymer electrolytes. *J. Am. Chem. Soc.* **127**, 4976–4983 (2005).
32. Kim, D. et al. Amine-functionalized boron nitride nanosheets: a new functional additive for robust, flexible ion gel electrolyte with high lithium-ion transference number. *Adv. Funct. Mater.* **30**, 1–9 (2020).
33. Chen, B. et al. Highly stretchable and transparent ionogels as nonvolatile conductors for dielectric elastomer transducers. *ACS Appl. Mater. Interfaces* **6**, 7840–7845 (2014).
34. Sharma, A. et al. Self-healing gelatin ionogels. *Int. J. Biol. Macromol.* **95**, 603–607 (2017).
35. Ajino, K. et al. Synthesis of ion-conductive polymers by radical polymerization of deep eutectic monomers bearing quaternary ammonium groups with urea. *Polymer* **204**, 122803 (2020).
36. Ribot, J. C. et al. Aqueous gelation of ionic liquids: reverse thermoresponsive ion gels. *Chem. Commun.* **46**, 6971–6973 (2010).
37. Tang, B. et al. Printable, degradable, and biocompatible ion gels from a renewable ABA triblock polyester and a low toxicity ionic liquid. *ACS Macro Lett.* **6**, 1083–1088 (2017).
38. Jeong, J. et al. Ink-jet printable, self-assembled, and chemically crosslinked ion-gel as electrolyte for thin film, printable transistors. *Adv. Mater. Interfaces* **6**, 1901074 (2019).
39. Chen, L. Y. et al. Cross-linked polymeric ionic liquids ion gel electrolytes by in situ radical polymerization. *Chem. Eng. J.* **378**, 122245 (2019).
40. Owyeung, R. E. et al. Highly flexible transistor threads for all-thread based integrated circuits and multiplexed diagnostics. *ACS Appl. Mater. Interfaces* **11**, 31096–31104 (2019).
41. Ko, J. et al. Self-healable electrochromic ion gels for low power and robust displays. *Org. Electron.* **71**, 199–205 (2019).
42. Park, B. J. et al. Pixel-free capacitive touch sensor using a single-layer ion gel. *J. Mater. Chem. C.* **7**, 10264–10272 (2019).
43. Hong, S. et al. A stretchable and compressible ion gel based on a deep eutectic solvent applied as a strain sensor and electrolyte for supercapacitors. *J. Mater. Chem. C.* **8**, 550–560 (2020).
44. Sato, T. et al. New design for a safe lithium-ion gel polymer battery. *J. Power Sources* **152**, 264–271 (2005).
45. Qin, B. et al. A single-ion gel polymer electrolyte system for improving cycle performance of $LiMn_2O_4$ battery at elevated temperatures. *Electrochim. Acta* **141**, 167–172 (2014).
46. Forsyth, M. et al. Innovative electrolytes based on ionic liquids and polymers for next-generation solid-state batteries. *Acc. Chem. Res.* **52**, 686–694 (2019).
47. Ma, X. F. et al. Photo-induced actuator using temperature and light dual responsive azobenzene containing ion gel in ionic liquid. *Eur. Polym. J.* **123**, 109446 (2020).
48. Imaizumi, S., Kokubo, H. & Watanabe, M. Polymer actuators using ion-gel electrolytes prepared by self-assembly of ABA-triblock copolymers. *Macromolecules* **45**, 401–409 (2012).
49. Seo, D. G. & Moon, H. C. Mechanically robust, highly ionic conductive gels based on random copolymers for bending durable electrochemical devices. *Adv. Funct. Mater.* **28**, 1706948 (2018).
50. Qian, C. et al. Flexible organic field-effect transistors on biodegradable cellulose paper with efficient reusable ion gel dielectrics. *RSC Adv.* **5**, 14567–14574 (2015).
51. Yoon, J. et al. Dye-sensitized solar cells using ion-gel electrolytes for long-term stability. *J. Power Sources* **201**, 395–401 (2012).
52. Kim, T. et al. Investigation on the ion-gel dielectric characteristics for graphene transistor toward flexible and transparent devices. *Sci. Adv. Mater.* **9**, 1589–1594 (2017).
53. Jiyoul Lee, L. G. K. et al. Ion gel-gated polymer thin-film transistors: operating mechanism and characterization of gate dielectric capacitance, switching speed, and stability. *J. Phys. Chem. C.* **113**, 8972–8981 (2009).
54. Lee, D. et al. Low voltage, high gain electrolyte-gated complementary inverters based on transfer-printed block copolymer ion gels. *Org. Electron.* **71**, 266–271 (2019).
55. Alquraishi, W. et al. Hybrid optoelectronic synaptic functionality realized with ion gel-modulated In_2O_3 phototransistors. *Org. Electron.* **71**, 72–78 (2019).
56. Lee, K. H. et al. "Cut and Stick" rubbery ion gels as high capacitance gate dielectrics. *Adv. Mater.* **24**, 4457–4462 (2012).
57. Lee, J. et al. Ion gel gated polymer thin-film transistors. *J. Am. Chem. Soc.* **129**, 4532–4533 (2007).

58. Sun, Q. et al. Active matrix electronic skin strain sensor based on piezopotential-powered graphene transistors. *Adv. Mater.* **27**, 3411–3417 (2015).

59. Jo, Y. J. et al. Biocompatible and biodegradable organic transistors using a solid-state electrolyte incorporated with choline-based ionic liquid and poly-saccharide. *Adv. Funct. Mater.* **30**, 1909707 (2020).

60. Cho, J. H. et al. Printable ion-gel gate dielectrics for low-voltage polymer thin-film transistors on plastic. *Nat. Mater.* **7**, 900–906 (2008).

61. Yomogida, Y. et al. Ambipolar organic single-crystal transistors based on ion gels. *Adv. Mater.* **24**, 4392–4397 (2012).

62. Zhang, S. et al. Ionic conductivity, capacitance, and viscoelastic properties of block copolymer-based Ion gels. *Macromolecules* **44**, 940–949 (2011).

63. Zhang, C. et al. Oxide synaptic transistors coupled with triboelectric nanogenerators for bio-inspired tactile sensing application. *IEEE Electron Device Lett.* **41**, 617–620 (2020).

64. Yu, F. et al. Artificial tactile perceptual neuron with nociceptive and pressure decoding abilities. *ACS Appl. Mater. Interfaces* **12**, 26258–26266 (2020).

65. Luo, J. et al. Double in-plane-gate IZO-based thin-film transistors with pea protein gate dielectrics. *J. Phys. D* **52**, 174001 (2019).

66. Wang, D. et al. Biomimetic, biocompatible and robust silk Fibroin-MXene film with stable 3D cross-link structure for flexible pressure sensors. *Nano Energy* **78**, 105252 (2020).

67. Yang, Y.-H. et al. Double-gate InZnO synaptic transistor with aqueous-solution-processed wheat flour electrolyte. *Org. Electron.* **77**, 105518 (2020).

68. Zhang, H. et al. Ion gel capacitively coupled tribotronic gating for multi-parameter distance sensing. *ACS Nano* **14**, 3461–3468 (2020).

69. Liu, J. et al. Fully stretchable active-matrix organic light-emitting electrochemical cell array. *Nat. Commun.* **11**, 3362 (2020).

70. Cong, H. et al. Multilayer graphene-GeSn quantum well heterostructure SWIR light source. *Small* **14**, e1704414 (2018).

71. Adinolfi, V. & Sargent, E. H. Photovoltage field-effect transistors. *Nature* **542**, 324–327 (2017).

72. Ran, W. et al. An integrated flexible all-nanowire infrared sensing system with record photosensitivity. *Adv. Mater.* **32**, e1908419 (2020).

73. Guo, Y. B. et al. Low-voltage protonic/photonic synergic coupled oxide phototransistor. *Org. Electron.* **71**, 31–35 (2019).

74. Kim, J. T. et al. Ion-gel-gated graphene optical modulator with hysteretic behavior. *ACS Appl. Mater. Interfaces* **10**, 1836–1845 (2018).

75. Yi, H. T. et al. Electric-field effect on photoluminescence of lead-halide perovskites. *Mater. Today* **28**, 31–39 (2019).

76. Liu, G., Jin, W. & Xu, N. Two-dimensional-material membranes: a new family of high-performance separation membranes. *Angew. Chem. Int. Ed. Engl.* **55**, 13384–13397 (2016).

77. Zheng, Z., Grunker, R. & Feng, X. Synthetic two-dimensional materials: a new paradigm of membranes for ultimate separation. *Adv. Mater.* **28**, 6529–6545 (2016).

78. Yao, B. et al. Gate-tunable frequency combs in graphene-nitride micro-resonators. *Nature* **558**, 410–414 (2018).

79. Lin, P. & Yan, F. Organic thin-film transistors for chemical and biological sensing. *Adv. Mater.* **24**, 34–51 (2012).

80. Lipomi, D. J. et al. Skin-like pressure and strain sensors based on transparent elastic films of carbon nanotubes. *Nat. Nanotechnol.* **6**, 788–792 (2011).

81. Wang, K. et al. Bioinspired interlocked structure-induced high deformability for two-dimensional titanium carbide (MXene)/natural microcapsule-based flexible pressure sensors. *ACS Nano* **13**, 9139–9147 (2019).

82. Wang, L. et al. High-performance, flexible electronic skin sensor incorporating natural microcapsule actuators. *Nano Energy* **36**, 38–45 (2017).

83. Sun, Q. et al. Transparent, low-power pressure sensor matrix based on coplanar-gate graphene transistors. *Adv. Mater.* **26**, 4735–4740 (2014).

84. Wang, X. et al. A sub-1V, microwatt power-consumption iontronic pressure sensor based on organic electrochemical transistors. *IEEE Electron Device Lett.* **42**, 46–49 (2021).

85. Wang, Z. L. Progress in piezotronics and piezo-phototronics. *Adv. Mater.* **24**, 4632–4646 (2012).

86. Wang, Z. L. Piezopotential gated nanowire devices: piezotronics and piezo-phototronics. *Nano Today* **5**, 540–552 (2010).

87. Wang, L. et al. Ultrathin piezotronic transistors with 2 nm channel lengths. *ACS Nano* **12**, 4903–4908 (2018).

88. Yeh, P. H., Li, Z. & Wang, Z. L. Schottky-gated probe-free ZnO nanowire biosensor. *Adv. Mater.* **21**, 4975–4978 (2009).

89. Wu, W., Wen, X. & Wang, Z. L. Taxel-addressable matrix of vertical-nanowire piezotronic transistors for active and adaptive tactile imaging. *Science* **340**, 952–957 (2013).

90. Pan, C. et al. High-resolution electroluminescent imaging of pressure distribution using a piezoelectric nanowire LED array. *Nat. Photonics* **7**, 752–758 (2013).

91. Kim, B. J. et al. High-performance flexible graphene field effect transistors with ion gel gate dielectrics. *Nano Lett.* **10**, 3464–3466 (2010).

92. Martins, P., Lopes, A. C. & Lanceros-Mendez, S. Electroactive phases of poly (vinylidene fluoride): determination, processing and applications. *Prog. Polym. Sci.* **39**, 683–706 (2014).

93. Sun, Q. et al. Piezopotential-programmed multilevel nonvolatile memory as triggered by mechanical stimuli. *ACS Nano* **10**, 11037–11043 (2016).

94. Zhou, T. et al. Syringe-injectable mesh electronics integrate seamlessly with minimal chronic immune response in the brain. *Proc. Natl Acad. Sci. USA* **114**, 5894–5899 (2017).

95. Choi, S. et al. Recent advances in flexible and stretchable bio-electronic devices integrated with nanomaterials. *Adv. Mater.* **28**, 4203–4218 (2016).

96. Wang, L. et al. Grain-boundary-induced drastic sensing performance enhancement of polycrystalline-microwire printed gas sensors. *Adv. Mater.* **31**, e1804583 (2019).

97. Wang, L. et al. Flexible, graphene-coated biocomposite for highly sensitive, real-time molecular detection. *Adv. Funct. Mater.* **26**, 8623–8630 (2016).

98. Wang, L. et al. Graphene-functionalized natural microcapsules: modular building blocks for ultrahigh sensitivity bioelectronic platforms. *Adv. Funct. Mater.* **26**, 2097–2103 (2016).

99. Wang, L. et al. Biocompatible and biodegradable functional polysaccharides for flexible humidity sensors. *Research* **2020**, 8716847 (2020).

100. Norton, J. J. et al. Soft, curved electrode systems capable of integration on the auricle as a persistent brain-computer interface. *Proc. Natl Acad. Sci. USA* **112**, 3920–3925 (2015).

101. Rivnay, J. et al. Organic electrochemical transistors. *Nat. Rev. Mater.* **3**, 17086 (2018).

102. Sekitani, T. et al. Ultraflexible organic amplifier with biocompatible gel electrodes. *Nat. Commun.* **7**, 11425 (2016).

103. Wustoni, S. et al. Enzyme-free detection of glucose with a hybrid conductive gel electrode. *Adv. Mater. Interfaces* **6**, 1800928 (2018).

104. Bihar, E. et al. A disposable paper breathalyzer with an alcohol sensing organic electrochemical transistor. *Sci. Rep.* **6**, 27582 (2016).

105. Minev, I. R. et al. Biomaterials. Electronic dura mater for long-term multimodal neural interfaces. *Science* **347**, 159–163 (2015).

106. Viventi, J. et al. Flexible, foldable, actively multiplexed, high-density electrode array for mapping brain activity in vivo. *Nat. Neurosci.* **14**, 1599–1605 (2011).

107. Viventi, J. et al. A conformal, bio-interfaced class of silicon electronics for mapping cardiac electrophysiology. *Sci. Transl. Med.* **2**, 24ra22 (2010).

108. Lee, H. et al. Ultrathin organic electrochemical transistor with nonvolatile and thin gel electrolyte for long-term electrophysiological monitoring. *Adv. Funct. Mater.* **29**, 1906982 (2019).

109. Park, S. I. et al. Soft, stretchable, fully implantable miniaturized optoelectronic systems for wireless optogenetics. *Nat. Biotechnol.* **33**, 1280–1286 (2015).

110. Rogers, J. A., Someya, T. & Huang, Y. Materials and mechanics for stretchable electronics. *Science* **327**, 1603–1607 (2010).

111. Mostafalu, P. et al. A toolkit of thread-based microfluidics, sensors, and electronics for 3D tissue embedding for medical diagnostics. *Microsyst. Nanoeng.* **2**, 16039 (2016).

112. LeCun, Y., Bengio, Y. & Hinton, G. Deep learning. *Nature* **521**, 436–444 (2015).

113. Wang, D. et al. Threshold switching synaptic device with tactile memory function. *Nano Energy* **76**, 105109 (2020).

114. Kuzum, D., Yu, S. & Wong, H. S. P. Synaptic electronics: materials, devices and applications. *Nanotechnology* **24**, 382001 (2013).

115. Ho, V. M., Lee, J.-A. & Martin, K. C. The cell biology of synaptic plasticity. *Science* **334**, 623–628 (2011).

116. Xie, D. et al. Coplanar multigate MoS_2 electric-double-layer transistors for neuromorphic visual recognition. *ACS Appl. Mater. Interfaces* **10**, 25943–25948 (2018).

117. Chen, C. et al. Visible-light ultrasensitive solution-prepared layered organic-inorganic hybrid perovskite field-effect transistor. *Adv. Opt. Mater.* **5**, 1600539 (2017).

118. Sun, F. et al. Bioinspired flexible, dual-modulation synaptic transistors toward artificial visual memory systems. *Adv. Mater. Technol.* **5**, 1900888 (2020).

119. Crone, B. et al. Large-scale complementary integrated circuits based on organic transistors. *Nature* **403**, 521–523 (2000).

120. Klauk, H. et al. Ultralow-power organic complementary circuits. *Nature* **445**, 745–748 (2007).

121. Xia, Y. et al. Printed sub-2 V gel-electrolyte-gated polymer transistors and circuits. *Adv. Funct. Mater.* **20**, 587–594 (2010).

122. Zare Bidoky, F. et al. Sub-3 V ZnO electrolyte-gated transistors and circuits with screen-printed and photo-crosslinked ion gel gate dielectrics: new routes to improved performance. *Adv. Funct. Mater.* **30**, 1902028 (2019).

123. Kingon, A. I., Maria, J. P. & Streiffer, S. K. Alternative dielectrics to silicon dioxide for memory and logic devices. *Nature* **406**, 1032–1038 (2000).

124. Naber, R. C. G. et al. Organic nonvolatile memory devices based on ferroelectricity. *Adv. Mater.* **22**, 933–945 (2010).

125. Sekitani, T. et al. Organic nonvolatile memory transistors for flexible sensor arrays. *Science* **326**, 1516–1519 (2009).
126. Koo, J. et al. Nonvolatile electric double-layer transistor memory devices embedded with Au nanoparticles. *ACS Appl. Mater. Interfaces* **10**, 9563–9570 (2018).
127. Kim, Y. et al. A bioinspired flexible organic artificial afferent nerve. *Science* **360**, 998–1003 (2018).
128. Yang, X. X. et al. Coupled ion-gel channel-width gating and piezotronic interface gating in ZnO nanowire devices. *Adv. Funct. Mater.* **29**, 1807837 (2019).
129. Park, S. et al. Sub-0.5 V highly stable aqueous salt gated metal oxide electronics. *Sci. Rep.* **5**, 13088 (2015).
130. Ha, M. et al. Aerosol jet printed, low voltage, electrolyte gated carbon nanotube ring oscillators with Sub-5 μs stage delays. *Nano Lett.* **13**, 954–960 (2013).
131. Bouchet, R. et al. Charge transport in nanostructured PS–PEO–PS triblock copolymer electrolytes. *Macromolecules* **47**, 2659–2665 (2014).
132. Thiburce, Q. et al. Nanoscale ion-doped polymer transistors. *Nano Lett.* **19**, 1712–1718 (2019).
133. Lu, G. et al. Realization of artificial synapse and inverter based on oxide electric-double-layer transistor gated by a chitosan biopolymer electrolyte. *Semicond. Sci. Technol.* **35**, 075014 (2020).
134. Robin, M. et al. Overcoming electrochemical Instabilities of printed silver electrodes in all-printed ion gel gated carbon nanotube thin-film transistors. *ACS Appl. Mater. Interfaces* **11**, 41531–41543 (2019).
135. Barbosa, M. S. et al. Tungsten oxide ion gel-gated transistors: how structural and electrochemical properties affect the doping mechanism. *J. Mater. Chem. C.* **6**, 1980–1987 (2018).
136. Lee, H. J. et al. Ultrahigh-mobility and solution-processed inorganic P-channel thin-film transistors based on a transition-metal halide semiconductor. *ACS Appl. Mater. Interfaces* **11**, 40243–40251 (2019).

ACKNOWLEDGEMENTS

AUTHOR CONTRIBUTIONS

D.P. Wang, Z. Lou, and G.Z. Shen designed the review, D.P. Wang, S.F. Zhao, and R.Y. Yin wrote the paper, D.P. Wang and L.L. Li organized references, Z. Lou, and G.Z. Shen supervised the project. All authors substantially contributed to research and reviewed the manuscript.

COMPETING INTERESTS

The authors declare no competing interests.

ADDITIONAL INFORMATION

Correspondence and requests for materials should be addressed to Z.L. or G.S.

Reprints and permission information is available at http://www.nature.com/reprints

Publisher's note Springer Nature remains neutral with regard to jurisdictional claims in published maps and institutional affiliations.